Towards an optimal antenna for helicon waves excitation

Ph. Guittienne[a] and E. Chevalier
HELYSSEN Sàrl, 24 Route du Pavement, 1018 Lausanne, Switzerland

Ch. Hollenstein
Centre de Recherches en Physique des Plasmas, Ecole Polytechnique Fédérale de Lausanne, 1015 Ecublens, Switzerland

(Received 20 December 2004; accepted 29 August 2005; published online 20 October 2005)

Helicon sources are known to produce high-density plasmas and have found many applications. Different types of antenna have been used for helicon excitation but none of them generate a radio-frequency (rf) field that matches the helicon wave field determined by the dispersion equation. We show that this match can be obtained to a very good approximation by using a birdcage type antenna. Our plasma experiments show that a helicon regime with electron densities up to 5×10^{12} cm^{-3} is obtained for very low rf power injection (typically 200 W), and at an unusual operating pressure up to 25 Pa. © *2005 American Institute of Physics*. [DOI: 10.1063/1.2081107]

I. INTRODUCTION

Helicon plasma sources have been extensively studied since the experiments performed by Boswell,[1] and appear to be very efficient for high-density (10^{12}–10^{13} cm^{-3}) plasma production with moderate power injection.[2] These plasma sources have a wide range of applications, including semiconductor manufacturing[3] and space-based thruster systems.[4] The microscopic processes leading to wave absorption and energy deposition are still not very well understood, especially for low-pressure discharges, and the optimization of a helicon plasma source remains a problem to be solved from this point of view. An approach for helicon plasma source improvement consists in helicon wave excitation optimization by means of specific antenna designs. Until now, only a few types of antenna have been developed: the more popular ones are Nagoya III antenna,[5] paddle-shaped antenna,[6] and helical antennas.[7] As proposed by Chen and co-workers,[7,8] the field generated by the rf antenna should match the helicon wave field as well as possible in order to optimize the wave excitation. Considering a specific helicon mode in a cylindrical geometry, it appears that the match between antenna and wave field can only be perfect if the antenna currents are distributed sinusoidally in the azimuthal direction (and also in z direction for an infinitely long antenna). This last assertion led us to the idea of using birdcage-type antennas for helicon plasma sources.[9]

II. HELICON WAVES

Helicon waves are electromagnetic waves that propagate in magnetized plasmas. In the frequency range $\omega_{ci}\ll\omega\ll\omega_{ce}$, the dispersion relation for a homogeneous cylindrical plasma without dissipation is given by[10,11]

$$\omega=\frac{kk_zB_0}{en_0\mu_0}, \tag{1}$$

where $\mathbf{k}=\mathbf{k}_\perp+\mathbf{k}_z$, $\mathbf{k}_\perp$ and $\mathbf{k}_z$ being the perpendicular and parallel components of the wave vector with regard to the direction of the static magnetic field $\mathbf{B}_0$, and n_0 is the electron density. Helicon waves are circularly polarized: the field quantities vary as $\exp[i(m\theta+k_zz-\omega t)]$ in a cylindrical coordinates system (r,θ,z) with the z axis aligned on $\mathbf{B}_0$. With $m=\pm1$, it means that for a given time the magnetic (or electric) wave field $\mathbf{B}(\theta,z)$ is transverse and its direction rotates linearly with z, as if it lies on a twisted flat tape.[7] The whole structure rotates with time around the z axis at frequency ω, the sense of rotation depending on the sign of m. It is conventional to denote by $m=1$ the right-hand polarization of the wave. The mode $m=1$ is of special interest as it appears experimentally to be the more efficient for plasma production compared to mode $m=-1$.[12,13]

III. THE BIRDCAGE-TYPE ANTENNA

A. Basic configuration

The birdcage-type antenna is well known in nuclear magnetic resonance (NMR) where it is commonly used as an excitation and detection device.[14] A schematic representation of a birdcage antenna is shown in Fig. 1. In a general description, the antenna is composed of N identical legs equally distributed on a cylinder of radius R. Each leg is connected at both ends to its two closest neighbors by means of capaci-

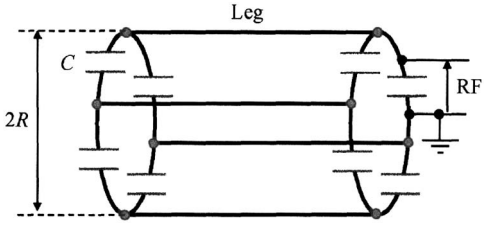

FIG. 1. Schematic representation of a 4-leg birdcage.

[a]Electronic mail: guittienne@helyssen.com

 © 2005 American Institute of Physics

Downloaded 09 Jul 2009 to 128.178.126.31. Redistribution subject to AIP license or copyright; see http://jap.aip.org/jap/copyright.jsp

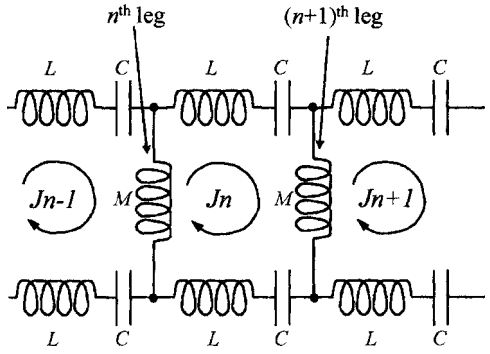

FIG. 2. Equivalent circuit of a segment of a birdcage antenna.

tors, usually of equal capacitance C. In its simplest design, the rf power is injected directly across one capacitor.

Considering the conducting parts of the antenna to act essentially as inductive components, the equivalent circuit of a segment of the antenna corresponds to the schema shown in Fig. 2, where M is the inductance of a single leg and L is the inductance of a portion of the capacitive ring. If we denote by J_n the loop current flowing in the loop defined by the nth leg and $(n+1)$th legs $(n=1,2,\ldots,N)$, we can write from Kirchhoff's voltage law the following expression:[14]

$$-i\omega M(J_n - J_{n-1}) - i\omega M(J_n - J_{n+1}) - 2i\omega L J_n + \frac{2i}{\omega C} J_n = 0,$$

$$\Rightarrow M(J_{n+1} + J_{n-1}) + 2\left(\frac{1}{\omega^2 C} - L - M\right) J_n = 0, \tag{2}$$

where ω is the excitation frequency. Because of the cylindrical symmetry, the current J_n must satisfy the periodic condition $J_n = J_{n+N}$. Therefore, the N independent solutions (*id.* modes) of Eq. (2) have the form,

$$(J_n)_{m_A} \propto \begin{cases} \cos\left(\dfrac{2\pi \cdot m_A n}{N}\right), & m_A = 0,1,\ldots,N/2, \quad \text{(3a)} \\ \sin\left(\dfrac{2\pi \cdot m_A n}{N}\right), & m_A = 1,2,\ldots,N/2-1, \quad \text{(3b)} \end{cases}$$

where $(J_n)_{mA}$ denotes the value of J_n in the m_Ath solution. The characteristic (resonant) frequency ω_{mA} for each mode is obtained by substituting Eq. (3a) or Eq. (3b) into Eq. (2) and has the following form:

$$\omega_{mA} = \left\{ C\left[L + 2M \sin^2\left(\frac{\pi m_A}{N}\right)\right]\right\}^{-1/2}, \tag{4}$$

$$m_A = 0,1,\ldots,N/2.$$

Note that choosing Eq. (3a) or Eq. (3b) leads to the same resonant frequency ω_{mA} for a given m_A. These two modes are called the degenerate modes and the rf fields they produce are just perpendicular to each other.

Finally, the rf current $(I_n)_{mA} = (J_n)_{mA} - (J_{n-1})_{mA}$ flowing in the nth leg under resonance at frequency ω_{mA} can be expressed in the following form:

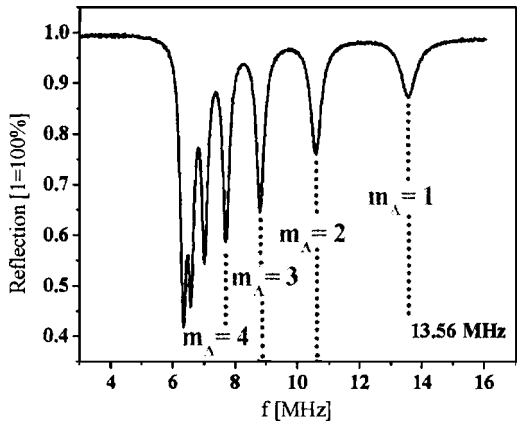

FIG. 3. Network analyzer measurement of the power reflection of a 16-leg unmatched birdcage as a function of the input signal frequency.

$$(I_n)_{mA} = I_0 \sin\left[\frac{\pi \cdot m_A}{N}\right] \sin\left\{\frac{2\pi \cdot m_A (n-1/2)}{N}\right\} \sin(\omega t), \tag{5}$$

$$m_A = 0,1,\ldots,N/2.$$

The resonant frequencies can be observed by network analyzer measurements. Figure 3 shows a power reflection measurement performed on a 16 leg unmatched antenna. Seven absorption peaks (modes 7 and 8 have very close frequencies) can be distinguished in the 6–14 MHz range, the highest frequency corresponding to the mode $m_A=1$. We have measured the current distributions in this antenna for the first 4 modes by means of an inductive current pickup, and found a very good agreement with the theoretical predictions (Fig. 4). Hence, with a sufficiently large number of legs, this antenna generates to a very good approximation a sinusoidal azimuthal current distribution, ideal for helicon wave excitation according to Chen and co-workers.[7,8]

The birdcage can be easily matched by a standard L-matching network[2] to the rf generator. An interesting fact is that under resonance the antenna has a purely real impedance, and is then already partially matched. For example, the antenna we used for our plasma experiments was measured

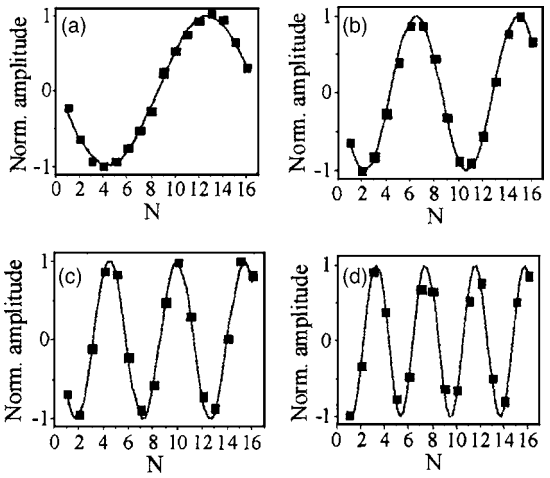

FIG. 4. Current distributions in a 16-leg birdcage measured by means of an inductive current pickup; full dots: measurements and line: theoretical. (a) $m_A=1$, (b) $m_A=2$, (c) $m_A=3$, and (d) $m_A=4$.

Downloaded 09 Jul 2009 to 128.178.126.31. Redistribution subject to AIP license or copyright; see http://jap.aip.org/jap/copyright.jsp

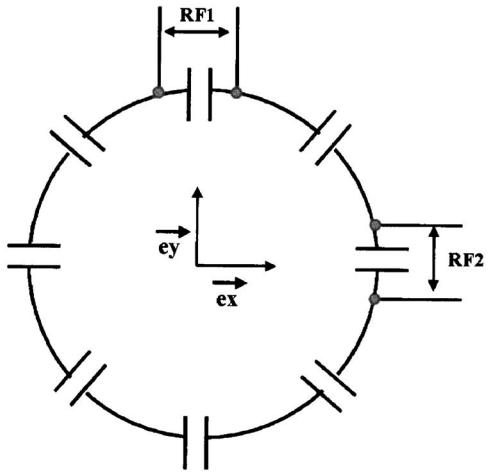

FIG. 5. Spatial phase quadrature feeding of a 8-leg birdcage.

to have a 30 Ω real impedance under resonance at 13.56 MHz (without plasma), the imaginary part being less than 1 Ω. With such values the matching network components need to support much lower currents than with usual antennas which generally present very high imaginary impedances and very low real impedances. This is of prime importance for minimizing the power losses due to dissipation in the matching network.

B. Quadratic feeding of the antenna

With the $m_A=1$ sinusoidal distribution of currents the birdcage generates a very homogeneous transverse linearly polarized rf field. This one can be seen as a superposition of left-hand and right-hand circularly polarized magnetic fields, which will couple equally to $m=1$ and $m=-1$ helicon modes. Hence, with this configuration half of the antenna's energy will be used for the $m=-1$ helicon mode generation, this being less efficient to heat the plasma than mode $m=1$.[12,13]

We now consider the configuration where the rf power is injected on two capacitors placed at 90° on the same capacitive ring, as schematically represented in Fig. 5. This does not affect the resonant properties of the antenna. At the same resonant frequency each source generates its own $m_A=1$ sinusoidal distribution of currents in the legs. In the situation represented in Fig. 5, rf1 generates a transverse linearly polarized rf field oriented along $\mathbf{e}_y$ while rf2 generates a transverse linearly polarized RF field oriented along $\mathbf{e}_x$. This configuration could be called a spatial phase quadratic feeding of the antenna, as we superpose two sinusoidal distributions of currents azimuthally shifted by a quarter of wavelength. As long as the two injected signals are temporally in phase the total rf field $\mathbf{B}_{\text{tot}}$ will remain linearly polarized. By imposing a 90 ° temporal phase shift between rf1 and rf2 signals (temporal phase quadrature), $\mathbf{B}_{\text{tot}}$ will have the following components:

$$\mathbf{B}_{\text{tot}} = B_0 \cos\{\omega t\} \cdot \mathbf{e}_x + B_0 \sin\{\omega t\} \cdot \mathbf{e}_y. \tag{6}$$

$\mathbf{B}_{\text{tot}}$ is a left-hand circularly polarized rf field as the $m=-1$ helicon mode. A −90° phase shift between rf1 and rf2 would lead to the $m=1$ right-hand circular polarization. Hence, the quadratic feeding of the birdcage allows all the antenna energy to be concentrated in the excitation of the most efficient helicon mode for plasma heating.

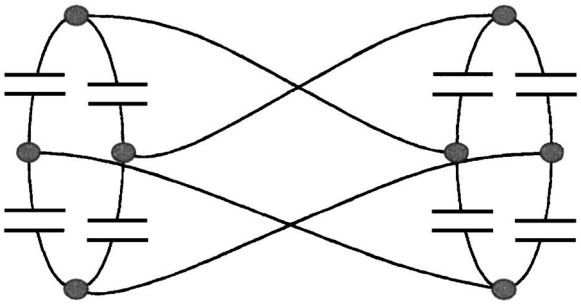

FIG. 6. Schematic representation of a 4-leg twisted birdcage.

C. Twisted antennas

An additional improvement in helicon-antenna field matching can be obtained by twisting the birdcage, as represented in Fig. 6. The currents in the legs remain sinusoidally distributed. Combined with the spatiotemporal quadratic excitation described above, the rf field generated by the twisted antenna will rotate both in time and along the longitudinal axis. The match between the antenna and the $m=1$ helicon wave field is then almost perfect, in the limit of finite antenna lengths.

In general, we expect the twisted birdcage to have a better inductive coupling with the plasma than a straight antenna. To demonstrate this point we model the currents in the legs of the birdcage as a sheet of continuous surface current on a cylindrical surface of radius R_0 and length L. In a cylindrical coordinate system (r,θ,z), with the z direction oriented along the static magnetic field, the modeled current density $\mathbf{J}(r,\theta,z)$ for a straight birdcage with a $m_A=1$ current distribution has the following components:[15]

$$J_r(r,\theta,z) = 0,$$

$$J_\theta(r,\theta,z) = \frac{I_0}{2R_0}\delta(r-R_0)\left[\delta\left(z+\frac{L}{2}\right)-\delta\left(z-\frac{L}{2}\right)\right] r\sin(\theta),$$

$$J_z(r,\theta,z) = \frac{I_0}{2R_0}\delta(r-R_0)\left[Y\left(z+\frac{L}{2}\right)-Y\left(z-\frac{L}{2}\right)\right]\cos(\theta), \tag{7}$$

where I_0 is a current, Y is the Heaviside function, and δ is the Dirac delta function. It has been shown[8,16] that the amplitude of the induced fields in the plasma is proportional to the azimuthal component of the Fourier transform of the antenna current distribution, $K_\theta(m,k_z)$, defined as

$$K_j(m,k_z) = \frac{1}{2\pi}\int_{-\infty}^{\infty} dz \int_0^{2\pi} d\theta J_j(r,\theta,z)\, e^{-i(m\theta+k_z z)}, \quad j=r,\theta,z. \tag{8}$$

Note that, by construction, the divergence of the antenna current distribution is zero everywhere, which means that there is a simple relation between $K_\theta(m,k_z)$ and the z component of the Fourier transform of the current distribution $K_z(m,k_z)$,[8]

Downloaded 09 Jul 2009 to 128.178.126.31. Redistribution subject to AIP license or copyright; see http://jap.aip.org/jap/copyright.jsp

$$K_z(m,k_z) = \frac{-m}{R_0 k_z} K_\theta(m,k_z). \tag{9}$$

Then $K_\theta(m,k_z)$ can be deduced from $K_z\,(m,k_z)$ which is much easily calculated. For the straight antenna, we obtain the following result for $K_\theta(m,k_z)$:

$$K_\theta(m,k_z) = \frac{I_0 e^{-im\pi}\sin(m\pi)}{(m^2-1)\pi}\sin\left(\frac{k_z L}{2}\right). \tag{10}$$

We see that $K_\theta(m,k_z)$ has a zero value for $m \neq \pm 1$, which just expresses the fact that all the antenna power will be used for the excitation of waves that have the $m=\pm 1$ azimuthal structure. Equation (10) then reduces to

$$K_\theta(\pm 1,k_z) = \frac{I_0}{2}\sin\left(\frac{k_z L}{2}\right). \tag{11}$$

We now consider a birdcage antenna twisted with an angle ϕ. For mathematical simplicity, we take the legs to be uniformly twisted, which means that at any point the tangent to a leg makes a constant angle α with respect to the z axis,

$$\alpha = \arctan\left(\frac{R_0\phi}{L}\right). \tag{12}$$

Then, the z component of the current density for the twisted antenna can be expressed as follow:

$$J_z(r,\theta,z) = \frac{I_0}{2R_0}\delta(r-R_0)\left[Y\left(z+\frac{L}{2}\right) - Y\left(z-\frac{L}{2}\right)\right] \times\cos\left(\theta - \frac{\phi z}{L}\right)\cos(\alpha). \tag{13}$$

As for the straight antenna, the Fourier transform $K_z\,(m,k_z)$ obtained by integration of Eq. (13) has a zero value for $m \neq \pm 1$. Then, after using Eq. (9), the final solution for $K_\theta(\pm 1,k_z)$ in the twisted antenna is given by

$$K_\theta(\pm 1,k_z) = \pm\frac{I_0 k_z L}{2(k_z L \pm \phi)\sqrt{1+[(R_0^2\phi^2)/L^2]}}\sin\left(\frac{k_z L \pm \phi}{2}\right). \tag{14}$$

Figure 7 shows the plots of $K_\theta^2(k_z)$, which can be seen to be proportional to the antenna power,[8] for $\phi=0$, $-\pi/2$, $-\pi$, $-3\pi/2$, with $R_0=5$ cm and $m=1$. For each twist angle the antenna length L has been adjusted in order to get the maximum of the first oscillation at the same value of k_z. This result is very similar to those obtained by Chen and Arnush[8] when comparing the power spectrum of helical antennas with Nagoya III straight antenna: the spectrum for a twisted birdcage is narrower and has a larger amplitude than for a straight one, which implies higher induced fields and therefore a better inductive coupling.

In addition, by designing an antenna with a freely adjustable twist, a fine tuning of k_z matching can be performed. In this case we consider that the length L_{leg} of a twisted leg is constant. Then, the effective length L of the antenna will depend on the twist angle,

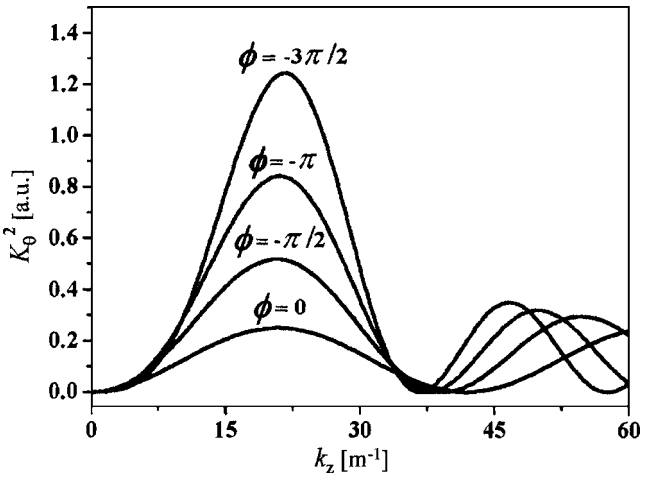

FIG. 7. Power spectrum for $\phi=0$, $-\pi/2$, $-\pi$, $-3\pi/2$, and $m=1$. The respective antenna lengths are $L=0.15$, 0.2, 0.25, and 0.3 m.

$$L = \sqrt{L_{\text{leg}}^2 - R_0^2\phi^2}. \tag{15}$$

In these conditions, there is an optimal twist angle ϕ_{opt} which maximizes the amplitude of $K_\theta^2(k_z)$ first oscillation. There is no analytical expression for ϕ_{opt} which has to be determined numerically. For example, with $L_{\text{leg}}=26$ cm and $R_0=5$ cm, an optimal value close to $(-\pi)$ is found for the twist angle, which leads to an effective length L of about 20 cm. By adjusting ϕ around the optimal value ϕ_{opt} we can significantly shift the antenna spectrum in k_z without substantially changing its amplitude (Fig. 8), which means that we can search for an optimal k_z value for given conditions (density, magnetic field, pressure,…).

IV. EXPERIMENTS

The plasma chamber is a 1.5-m-long quartz tube with an internal diameter of 9 cm (Fig. 9). The tube is centred in a 14 coil magnet (35 cm in diameter) extending over 1 m. The coils generate static fields up to 800 G. The pumping system reaches an ultimate pressure of 0.5 Pa. The antenna is a 16 leg straight birdcage, 27 cm in length and 11 cm in diameter, with a single rf power injection. It contains 32 high

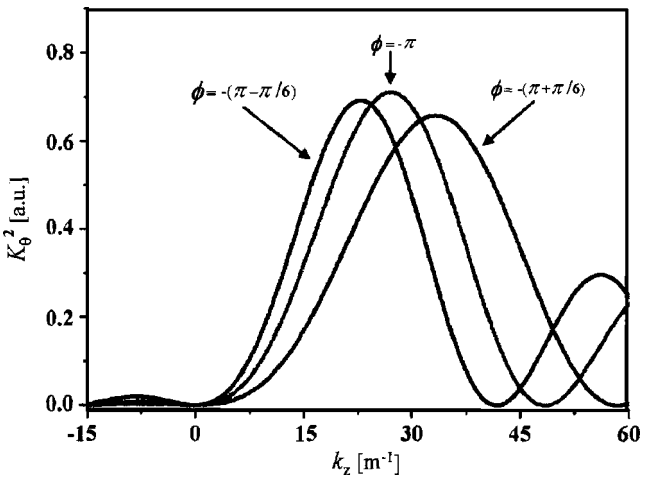

FIG. 8. Effect of an adjustable twist on the birdcage antenna power spectrum.

Downloaded 09 Jul 2009 to 128.178.126.31. Redistribution subject to AIP license or copyright; see http://jap.aip.org/jap/copyright.jsp

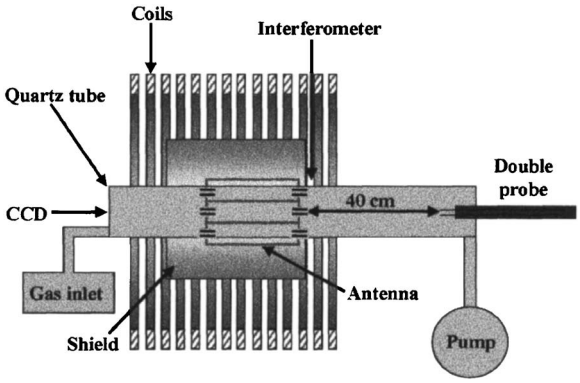

FIG. 9. Experimental setup.

current, high Q, nonmagnetic capacitors, each having a capacitance of 3.7 nF. The antenna is coaxial with the tube and surrounded by a copper electrostatic shield (30 cm long and 22 cm in diameter). For optimal performances the antenna has to resonate at the rf generator excitation frequency (13.56 MHz). But, depending on plasma's density and shape, the antenna $m_A=1$ resonant frequency will be slightly increased by typically 100 kHz. This effect is corrected by adjusting the position of the shield with respect to the antenna. A rf output power of 500 W is available.

A 33 GHz interferometer is used to measure the plasma density at one end of the antenna (Fig. 9). This method is one of the most reliable for plasma density determination, although it only gives a line-integrated electron density. We also use a double Langmuir probe to measure the electron temperature and the ion density in the center of the discharge tube. The probe can be moved longitudinally over 40 cm from the end of the antenna (Fig. 9). Finally we have a visual monitoring of the discharge by means of a charge-coupled device (CCD) camera showing the plasma through a glass window at the end of the quartz chamber (Fig. 9).

The results we present here concern discharges with argon, although similar results have been obtained with other noble gases (He, Ne, and Xe) and with SF_6. The experiments were performed for applied magnetic fields between 300 and 800 G and with filling pressures between 2 and 25 Pa. It has to been mentioned that a 25 Pa operating pressure is at least ten times higher than the one usually used in helicon discharges.

Figure 10 shows the static measurements of the electron density as a function of the injected rf power performed by microwave interferometry ($B_0=700$ G and pressure of 8 Pa). The open circles represent the electron density measured during the increasing power ramp while the closed circles represent the electron density measured during the decreasing power ramp. The plasma is ignited at a low rf power of typically 40 W. From 40 to 300 W the electron density is low ($<2\times10^{11}$ cm^{-3}) and increases linearly with the injected power. At 320 W a big jump in the electron density is observed, up to 4×10^{12} cm^{-3} (assuming a flat radial plasma profile). After the jump, the density remains approximately constant even if the power is increased up to 500 W. This high-density regime is maintained when the power is decreased, until it reaches 80 W whereupon the discharge goes back to the low-electron-density regime.

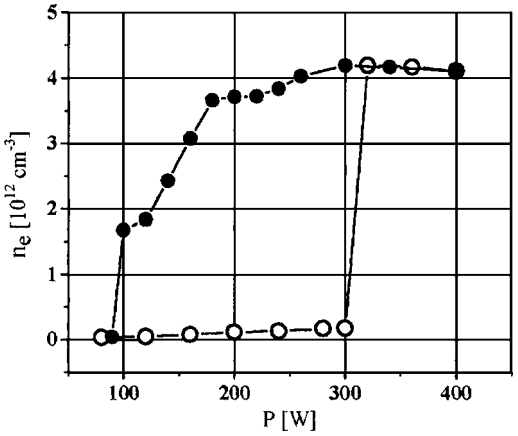

FIG. 10. Measurement of the plasma density during an up-down power ramp cycle (up: open circles and down: close circles), performed by 33 GHz interferometry at the antenna end.

The double probe was used to estimate the electron temperature T_e, which was found to be 4 ± 0.5 eV in the high-electron-density regime. The probe saturation current was used for ion density measurements along the axis of the discharge tube. Figure 11 shows two static measurements of the ion density during a 40–400 W power cycle ($B_0=700$ G and pressure of 13.5 Pa). One measurement was performed at the antenna end and the other at 25 cm from the antenna's end. At 280 W a big jump of the density is observed at the end of the antenna, but which is almost not detectable at 25 cm. As the power is lowered, the density stays more or less constant until a power of 180 W is reached for which another regime transition is observed. It corresponds to a plasma longitudinal extension, which can be seen by the sudden increase of the saturation current at 25 cm. This elongated regime is maintained until a 80 W power is reached. At that point no more current is measured at 25 cm but a quite high ion density persists at the antenna end. This last regime is maintained down to 50 W, after which the plasma returns to a low-density regime.

Qualitative explanations of these results can be given by observation of the plasma emission by means of the CCD camera. In the first part of the power ramp, which is in the

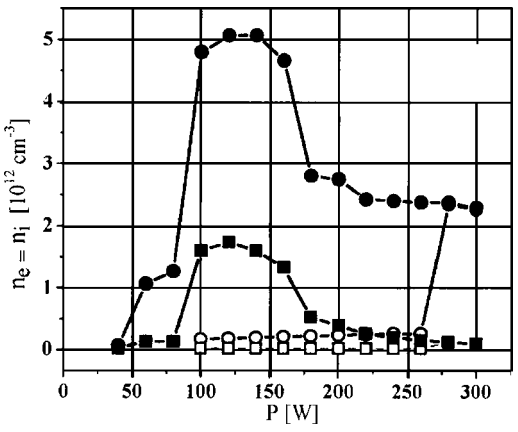

FIG. 11. Probe measurements of the plasma density as a function of the injected power. The measurements were performed at the antenna's end (open and close circles) and at 25 cm from the antenna's end (open and closed squares).

Downloaded 09 Jul 2009 to 128.178.126.31. Redistribution subject to AIP license or copyright; see http://jap.aip.org/jap/copyright.jsp

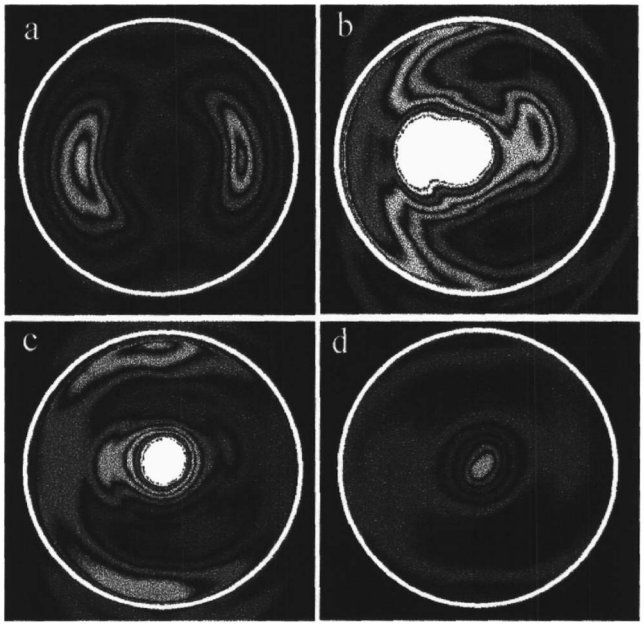

FIG. 12. CCD pictures of an Ar discharge (13 Pa and 700 G) (a) low-density regime with capacitive inductive coupling, (b) transition to helicon coupling, (c) transition to elongated helicon regime, and (d) centered regime maintained down to 50 W.

low-electron-density regime, the plasma is generated on the side of the chamber [Fig. 12(a)]. The "bean" shapes correspond to the sinusoidal current distribution in the antenna's legs and the discharge is driven by capacitive and inductive couplings. For an injected rf power of 280 W, a critical electron density is reached and the transition to the high-density regime occurs. The plasma distribution changes drastically [Fig. 12(b)] and the discharge is now sustained from the center of the tube. Such heating at the center is typical of helicon discharges.[17] When the rf power is lowered the plasma does not change much until a 160 W power is reached and the elongated regime suddenly takes place. The plasma is now very well centered and looks very cylindrical [Fig. 12(c)]. These measurements suggest that a good helicon coupling is obtained. Centred cylindrical regimes are maintained down to 50 W [Fig. 12(d)].

V. CONCLUSION

In this paper we showed that a birdcage-type antenna is theoretically ideal for specific helicon mode excitation, the more interesting one being the mode $m=1$ regarding plasma heating. A twisted birdcage with power injection in spatiotemporal phase quadrature generates a rf field that matches exactly the $m=1$ helicon wave field. To test the potential of this antenna type, we performed a set of experiments with a straight 16 leg antenna and without phase quadratic feeding. This antenna generates a very homogeneous transverse linearly polarized rf field due to the sinusoidal azimuthal distribution of current in the antenna legs. Two-dimensional (2D) imaging of the discharge shows that helicon regimes are obtained for very low-power injection (typically 200 W), and can be maintained down to 50 W. Average plasma densities up to 5×10^{12} cm^{-3} have been measured by 33 GHz interferometry at the outlet of the plasma source. A striking result is that these helicon regimes are obtained under very high pressures (2–25 Pa) compared to usual operating pressures of about 1 Pa, which is of great interest for industrial applications which often require high-pressure processes.

ACKNOWLEDGMENTS

We thank the EPFL and all other partners for supplying our test benchmark equipment. We gratefully thank F. F. Chen for his comments and valuable discussions.

[1] R. W. Boswell, Plasma Phys. Controlled Fusion **26**, 1147 (1984).
[2] M. A. Lieberman and A. J. Lichtenberg, *Principles of Plasma Discharges and Material Processing* (Wiley-Intersciences, New York, 1994).
[3] A. J. Perry, D. Vender, and R. W. Boswell, J. Vac. Sci. Technol. B **9**, 310 (1991).
[4] F. R. Chang Diaz *et al.*, *Proceedings 36th AIAA/ASME/ASEE Joint Propulsion Conference*, 2000 (unpublished), No 2000-3756.
[5] T. Watari *et al.*, Phys. Fluids **21**, 2076 (1978).
[6] R. W. Boswell, Phys. Lett. **33A**, 457 (1970).
[7] D. G. Miljak and F. F. Chen, Plasma Sources Sci. Technol. **7**, 61 (1998).
[8] A. Arnush and F. F. Chen, Phys. Plasmas **5**, 1239 (1998).
[9] Ph. Guittienne and E. Chevalier, Patent No. EP03405360.3 (2003).
[10] F. F. Chen and D. Arnush, Phys. Plasmas **4**, 3411 (1997).
[11] F. F. Chen, Plasma Phys. Controlled Fusion **33**, 339 (1991).
[12] F. F. Chen *et al.*, Plasma Sources Sci. Technol. **5**, 173 (1996).
[13] K. Suzuki, K. Nakamura, and H. Sugai, Jpn. J. Appl. Phys., Part 1 **35**, 4044 (1996).
[14] Jianming Jin, *Electromagnetic Analysis & Designs in Magnetic Resonance Imaging* (CRC, Boca Raton, FL, 1998).
[15] J. Pictet *et al.*, Phys. Med. Biol. **47**, 2973 (2002).
[16] K. P. Shamrai and B. V. Taranov, Plasma Sources Sci. Technol. **5**, 474 (1996).
[17] D. D. Blackwell and F. F. Chen, Plasma Sources Sci. Technol. **6**, 569 (1997).

Downloaded 09 Jul 2009 to 128.178.126.31. Redistribution subject to AIP license or copyright; see http://jap.aip.org/jap/copyright.jsp